JOURNAL OF MATERIALS SCIENCE 26 (1991) 4484–4490

Pressureless sintering and mechanical properties of alumina-sialon composites

K. TAKATORI
Toyota Central Research and Development Labs., Inc., 41-1 Aza Yokomichi, Oaza Nagakute, Nagakute-cho, Aichi-gun, Aichi-ken, 480-11 Japan

Compositions of Al_2O_3, Si_3N_4 and AlN were sintered to produce six different alumina-sialon composites. The composites reached the highest density at 1700 °C in a nitrogen atmosphere. Sialon acted as a binder, promoting the densification and suppressing the grain growth of alumina. The composites had a bending strength of 450 MPa at room temperature and maintained high strength over 300 MPa at 1400 °C. The composite with 30 wt % sialon had the maximum fracture toughness of 4.3 MPa·$m^{1/2}$ and exhibited good oxidation resistance even at 1400 °C. Mullite was formed in the oxidation layer and little degradation in strength was observed after oxidation.

1. Introduction

Alumina is one of the most important materials in the engineering field. A large amount of the material is used, for example, in spark plugs for automobile engines, IC substrates and cutting tools. Its chemical stability is widely used in high temperature structural components, while non-oxide ceramics such as Si_3N_4 have a serious problem of oxidation damage at high temperatures [1]. As for the strength of alumina, it gradually decreases at high temperatures, probably due to its ionic bonding nature. Hot-pressed composites of alumina and sialon have been studied to improve the strengths at high temperatures [2, 3]. Sialon was synthesized during the sintering of the composites through the reaction of Si_3N_4, AlN and alumina. The composites kept higher strength up to 1400 °C than single phase alumina ceramics.

This paper describes the results of pressureless sintering of alumina-sialon composites and the evaluation of their mechanical properties. The relations between the microstructures of composites and their mechanical properties are also discussed.

2. Experimental procedure

Table I shows the compositions of the starting powders. The numbers in the sample names indicate the initial weight percentages of alumina in individual samples. The weight ratios of Si_3N_4 and AlN were determined to synthesize β-sialon of $z = 2$ ($Si_{6-z}Al_zO_zN_{8-z}$), assuming the following reaction.

$$4Si_3N_4 + 2AlN + 2Al_2O_3 \rightarrow 3Si_4Al_2O_2N_6$$

The oxygen contents in Si_3N_4 and AlN were disregarded in the weight calculation. The "nominal" sialon contents that will be synthesized during sintering are also shown in Table I. The starting powders were mixed for 20 hours in a polyethylene container using nylon-coated iron balls and ethyl alcohol as a mixing fluid. The resultant slurry was dried and sifted for cold pressing. The powders were compacted by die pressing and then by cold isostatic pressing under a pressure of 300 MPa.

Pressureless sintering was executed in a graphite heat element furnace in a nitrogen atmosphere. The powder compacts were mounted in a boron nitride container. They were constantly sintered for 2 hours under 5 soaking temperatures from 1500 to 1800 °C. Nitrogen gas pressure was raised to 1 MPa at 1800 °C to prevent the decomposition of nitrides.

The specimens sintered at 1700 °C for 2 hours were cut into rectangular bars for mechanical property measurements. The bars were ground to a sample size of 3 by 4 by 40 mm with a 600-grid diamond wheel along the longitudinal direction. The edges were bevelled. The following properties were examined:

1. Crystalline phase. α-alumina and β-sialon were identified by X-ray diffraction analysis (XRD). No other crystalline phases were detected.
2. Microstructure. Fractured surfaces and selectively etched surfaces were observed by SEM.
3. Bending strength. 4-point bending strengths were measured in air at room temperature, and in vacuum at 1200 and 1400 °C. The inner and outer spans were 10 and 30 mm, respectively. The cross head speed was set at 0.5 mm min^{-1} [4].
4. Young's modulus and Poisson's ratio: Static properties were measured by 4-point bending tests using a crossed strain gauge. The specimens were thinned to a thickness of 1.5 mm for the measurement.
5. Hardness. Vicker's hardness was measured under 196 N loading.
6. Fracture toughnes. Fracture toughness (K_{IC}) was measured by an indentation technique under 196 N loading. K_{IC} was calculated using Niihara's equation for the median crack [5].

0022–2461/91 $03.00 + .12

TABLE I Compositions of starting powders and nominal sialon contents

Sample name	Compound (wt %)			Nominal sialon content (wt %)
	Al_2O_3[a]	Si_3N_4[b]	AlN[c]	
A100	100	0	0	0
NA99	99	0.87	0.13	1.3
NA95	95	4.37	0.63	6.6
NA90	90	8.73	1.27	13.2
NA80	80	17.5	2.54	26.3
NA60	60	34.9	5.09	52.7
NA40	40	52.4	7.64	79.0

[a] Iwatani Kagaku Co. Ltd., Japan, SAI, Purity 99.9%. Average particle size (p.s.) 0.6 μm.
[b] Ube Industries Ltd., Japan, SN-EIO (p.s.) 0.2 μm.
[c] Tokuyama Soda Co. Ltd., Japan, F-grade (p.s.) 0.5 μm.

7. Oxidation. The specimens were kept at 1400 °C in static air for 50, 150 and 500 hours. Three specimens were examined for each condition. Weight changes, crystalline phases, microstructures and bending strengths after oxidation were studied.

3. Results and discussion

3.1. Densification

Fig. 1 shows the relation between the specific gravities of the sintered composites and the soaking temperatures. Pure alumina (A100) densified to its highest specific gravity of 3.94 at 1700 °C. The alumina-sialon composites also reached their maximum densities at 1700 °C. NA99 and NA95 began to densify at lower temperatures than A100. This indicates that small amounts of Si_3N_4 and AlN play an important role as densification additives. The densities of all the specimens sintered at 1800 °C were lower than those sintered at 1700 °C. The weight losses of the specimens sintered at 1800 °C, especially for high sialon content specimens, were much more than those sintered at 1700 °C. These facts indicate that the decrease in density at 1800 °C was caused by the decomposition of sialon.

The specific gravity of a fully dense alumina-sialon composite should decrease as the content of sialon increases, because the specific gravity of sialon is about 20% less than that of alumina. Fig. 2 shows the relation between the specific gravities of sintered composites and their sialon content. The theoretical value is also shown in Fig. 2 by an interrupted line. The sialon contents in the composites were experimentally evaluated by the XRD method. The specific gravity of the composite decreased with a larger gradient than the theoretical line, indicating the retardment of densification due to a large amount of sialon.

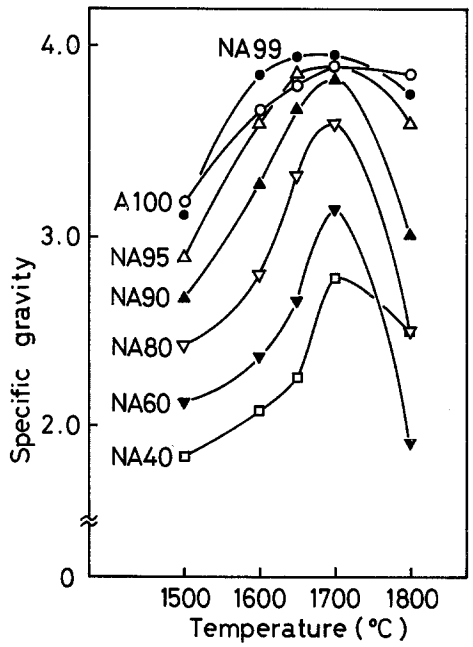

Figure 1 Densification profiles of alumina-sialon composites and pure alumina in nitrogen atmosphere.

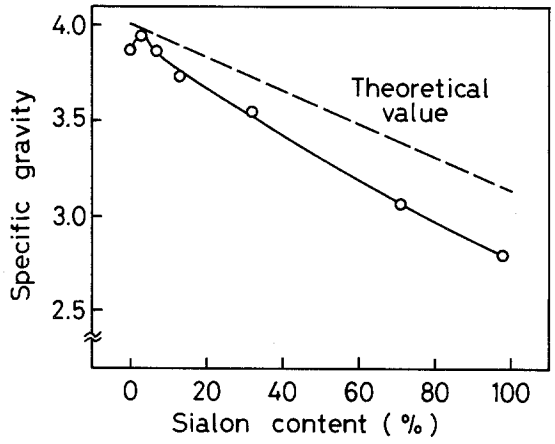

Figure 2 Relation between specific gravity and sialon content of composites sintered at 1700 °C.

TABLE II Content and z-value of sialon in composites sintered at 1700 °C

Sample name	Sialon[a] content (wt %)	z-Value
A100	0	–
NA99	3	2.5
NA95	7	2.5
NA90	13	2.5
NA80	32	2.6
NA60	71	3.1
NA40	98	2.9

[a] Sialon (2 0 0)/(sialon (2 0 0) + alumina (1 1 3)) × 100

3.2. Crystalline phase

Table II shows the contents of sialon obtained by experiment and its z-values evaluated by the XRD method. The sialon content was calculated from the peak heights of alumina (1 1 3) and sialon (2 0 0). For A100–NA80, the experimental sialon contents shown in Table II are in good agreement with the nominal ones shown in Table I. However, the experimental values for NA60 and NA40 are about 20% higher than nominal ones. It is noteworthy that these two samples contained sialons with about 0.5 higher z-values than the intended ones. A component corresponding to Al_3O_3N (Al_2O_3 + AlN) and Si_3N_4 are necessary to synthesize a sialon, which has volume

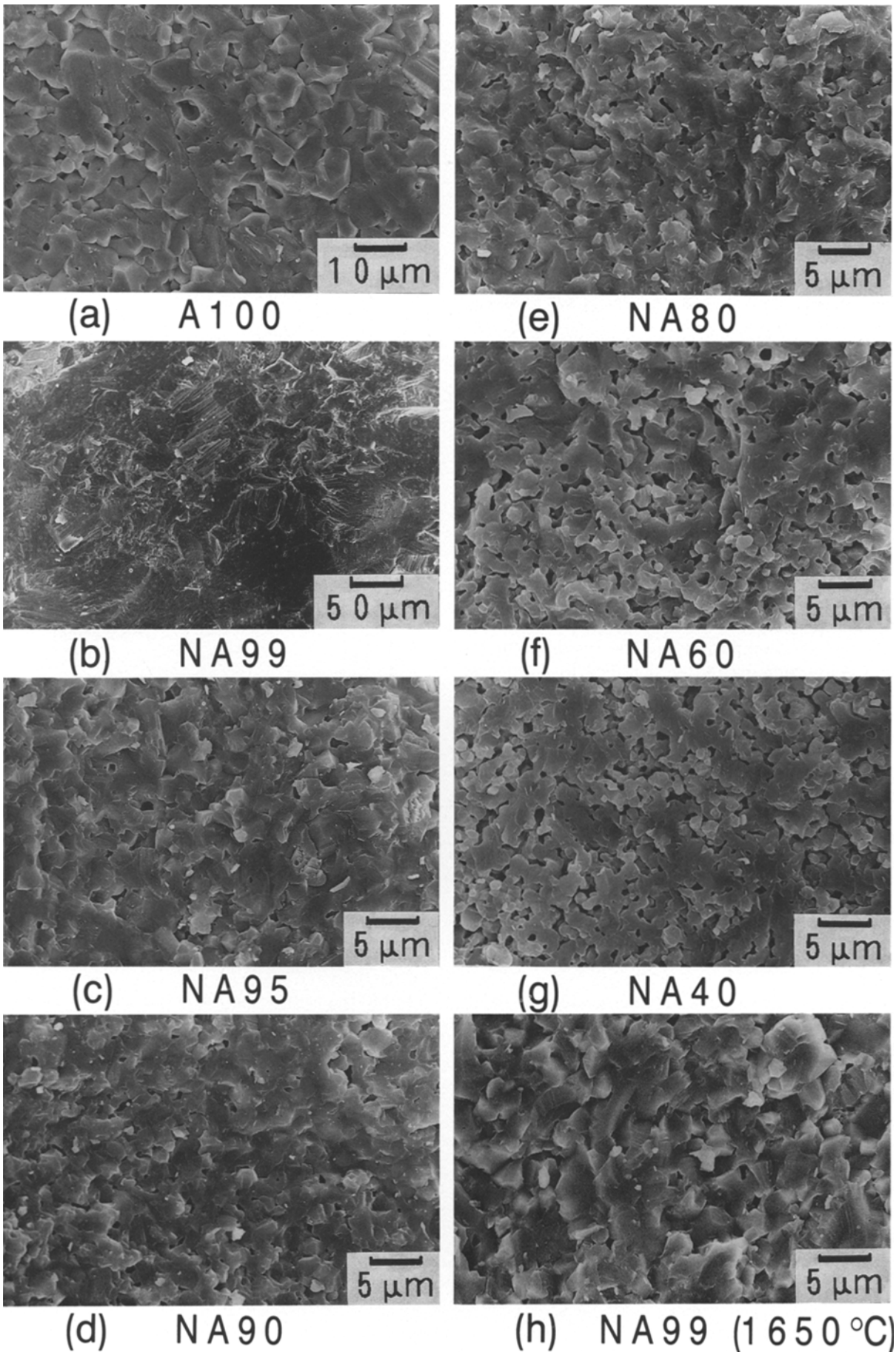

Figure 3 Fracture surfaces of alumina-sialon composites.

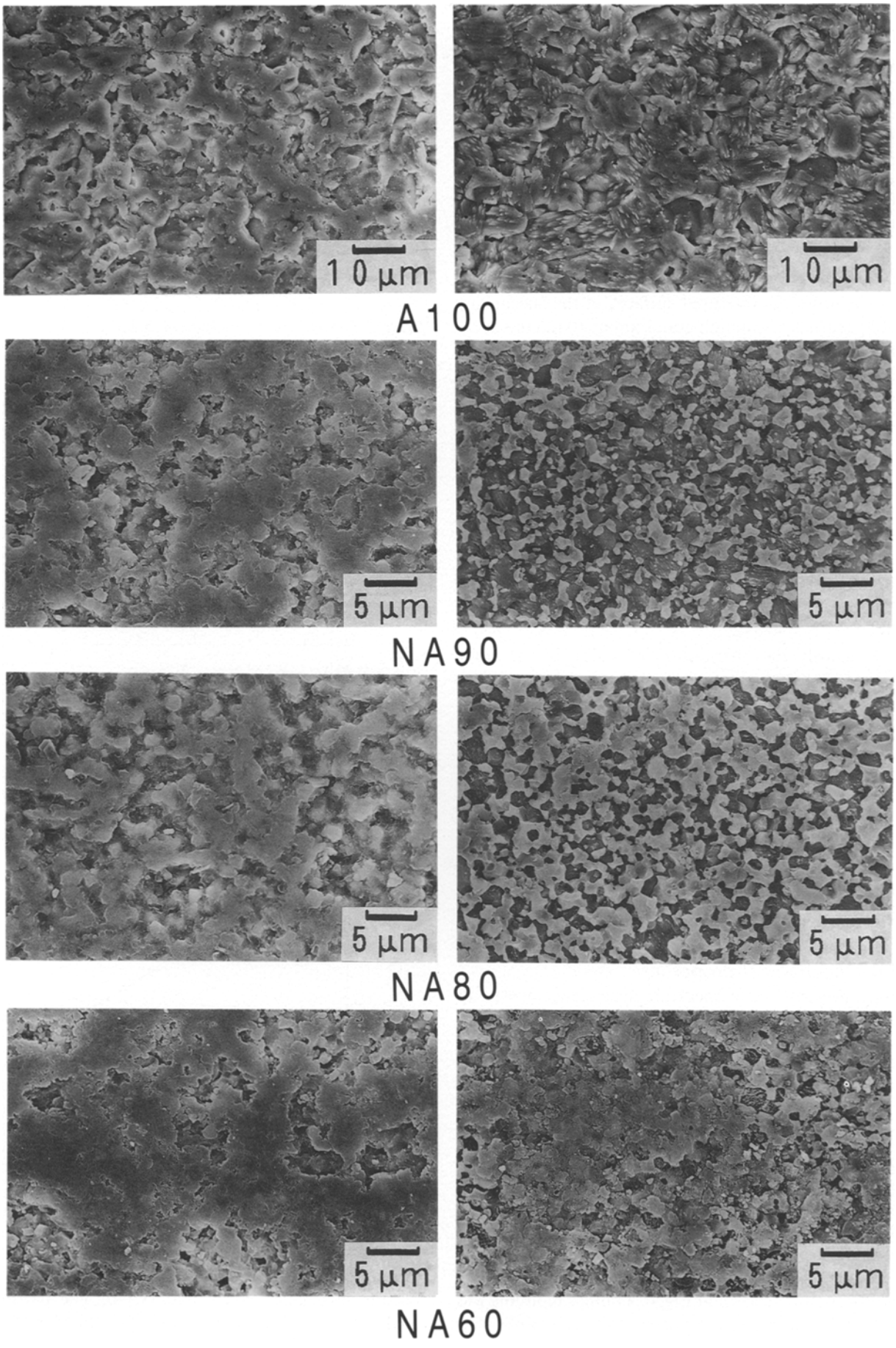

Figure 4 Ground surfaces (left) and etched surfaces (right) of alumina-sialon composites. Alumina was selectively removed from the ground surfaces.

fractions controlling the z-value and the amount of sialon. The high z-values of the two composites are considered to be caused by the synthesis of a large amount of Al_3O_3N by partial nitridation of alumina during sintering. The nitridation process is considered to be accelerated through the remaining open pores of NA60 and NA40. Neither nitride nor oxynitride were detected by XRD for A100. It is considered, therefore, that the nitridation of alumina was induced by the catalytic effect of Si_3N_4 or sialon.

3.3. Microstructure

Fig. 3 shows the fractured surfaces of the specimens. A100 consists of alumina grains about 10 μm in size. A small amount of pores are located in the grains and in the intergranular sites. The grains of NA99, which could be densified at a lower temperature than A100, remarkably grew up to about 50 μm generating numerous micro-pores. Another NA99 specimen sintered at 1650 °C is presented in Fig. 3h, whose exaggerated grain growth was restrained to an average grain size of about 3 μm. In other specimens from NA95 to NA40, the grain growth was restrained at the sintering condition of 1700 °C; the grain size decreased with increasing nitride content. It is impossible to distinguish between sialon and alumina grains in Fig. 3.

To clarify the distribution of sialon in the composites, the composites were heat treated in a graphite container at 1400 °C in a vacuum for selective etching of alumina; alumina decomposes and evaporates at this condition whereas sialon remains. Fig. 4 shows the ground surfaces before and after the heat treatment. The morphology of sialon changed from isolated intergranular grains to a continuous matrix as the sialon content increased. Sialon seems to act as a binder of alumina particles, suggesting that sialon promotes densification of alumina, forming a liquid phase.

3.4. Mechanical properties

Fig. 5 presents the temperature dependence of 4-point bending strength of the composites. The strengths of the composites NA95–NA80 at room temperature were about 450 MPa, 200 MPa higher than that of A100. However, the strength of NA60 and NA40 at room temperature were lower because the densities of these composites were not high enough. NA95–NA80 kept high strength over 300 MPa at 1400 °C. The proportion of the strength at 1400 °C against that at room temperature increases with the sialon content in the composites; the proportions of A100, NA90 and NA60 were 55%, 71% and 88%, respectively.

Static Young's modulus and Poisson's ratio of the composites are shown in Fig. 6. Young's modulus was relatively low due to the existence of some pores. The maximum value for NA99 was unobtainable, probably attributable to its extraordinary microstructure. Poisson's ratio, which was 0.23, did not depend on the composition.

The relation between Vicker's hardness, H_V and the sialon content is shown in Fig. 7. The composites

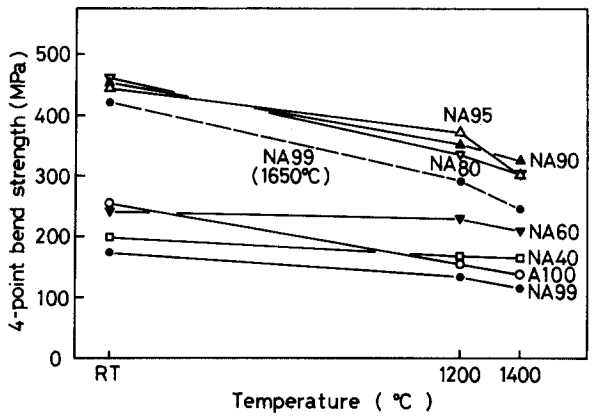

Figure 5 Temperature dependence of bending strength of the composites.

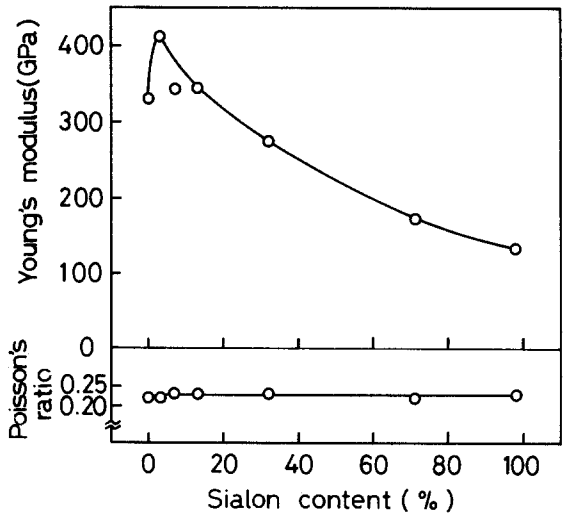

Figure 6 Young's modulus and Poisson's ratio of composites.

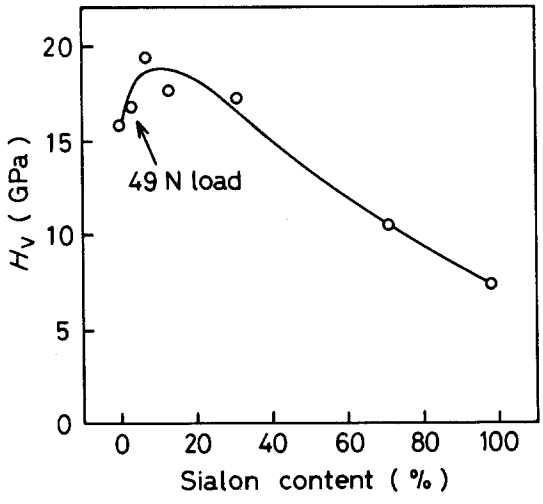

Figure 7 Composition dependence of Vicker's hardness, H_V, of the composites.

exhibited higher hardness than A100, except for the porous specimens, NA60 and NA40. The hardness could not be measured under 196 N loading for NA99, because the impression was desperately damaged by lateral cracking. The hardness of NA99 presented in Fig. 7 was measured using the impression indented under 49 N loading.

Fig. 8 shows the K_{IC} of the composites. The composites have the maximum K_{IC} value of

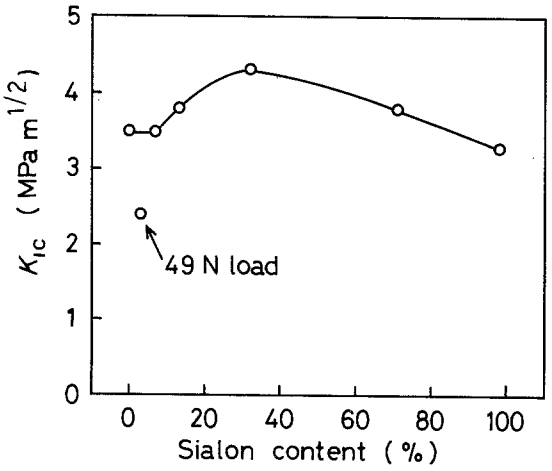

Figure 8 Composition dependence of the fracture toughness, K_{IC}, of composites.

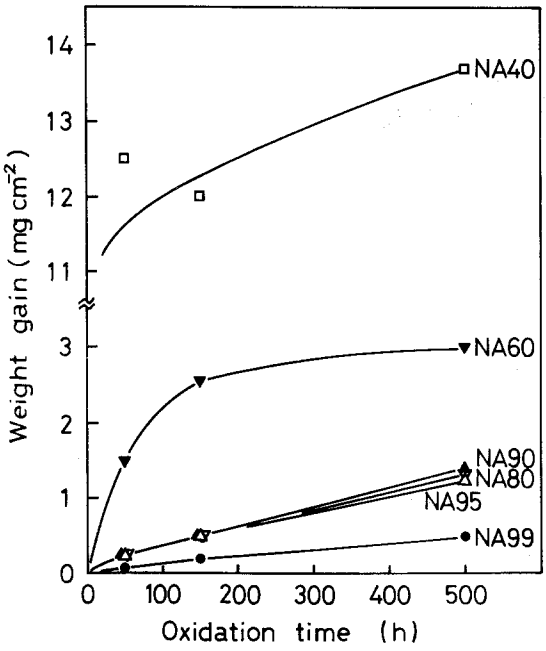

Figure 9 Time dependence of oxidation weight gain of composites at 1400 °C.

4.3 MPa·m$^{1/2}$, which is 20% higher than that of A100 (K_{IC} = 3.5 MPa·m$^{1/2}$. The maximum was obtained with 30 wt % sialon, corresponding to the continuous network formation of an intergranular sialon phase. The K_{IC} of NA99 measured under 49 N loading was exceptionally low as 2.4 MPa·m$^{1/2}$. Further detailed experiments are necessary to comprehend and control the K_{IC} of the composites.

3.5. Oxidation

Fig. 9 shows the weight gain of the composites after oxidation at 1400 °C. The weight gains were less than 1.4 mg·cm^{-2} even after 500 hours, except for the porous specimens, NA60 and NA40.

Crystalline phases of the surfaces after oxidation were identified by XRD as presented in Table III. For the specimens NA99–NA90, alumina was the dominant phase and mullite instead of sialon was detected on the oxidation surfaces. The diffraction peak intensity of mullite increased with oxidation duration for all specimens. Glass formation in the oxidation layer was

TABLE III Crystalline phases after oxidation at 1400 °C

Sample name	Before oxidation	50 h	150 h	500 h
A100	A	–	–	A
NA99	A ≫ SA	A ≫ M	A ≫ M	A ≫ M
NA95	A ≫ SA	A ≫ M	A ≫ M	A ≫ M
NA90	A ≫ SA	A > M	A > M	A > M
NA80	A > SA	M > A ≫ SA	M > A	M > A
NA60	SA > A	M ≫ SA ~ A Glass	M Glass	M Glass
NA40	SA ≫ A	M ≫ A Glass	M Glass	M Glass

A Al_2O_3; SA sialon; M $3Al_2O_3 \cdot 2SiO_2$

observed in the XRD profiles of NA60 and NA40. The sample surfaces lost their gloss and the original grey colour faded to white after oxidation.

Fig. 10 shows the representative microstructures of the oxidation layers. It indicates the cross sections and surface of specimen NA80 after 500 hours of oxidation. The oxidation layer thickness was about 75 μm. The layer can be clearly distinguished from the matrix because of the numerous micro-openings generated inside. The oxidation of sialon with $z = 2.5$ coexisting with alumina reacts as follows:

$$4Si_{3.5}Al_{2.5}O_{2.5}N_{5.5} + 16Al_2O_3 + 16.5O_2 \rightarrow 7(3Al_2O_3 \cdot 2SiO_2) + 11N_2 \uparrow$$

Micro-openings are considered to be formed by the production of nitrogen gas. The dominant sialon phases were oxidized forming glassy surface layers for NA60 and NA40, because a relatively small amount of alumina was insufficient to form stoichiometric mullite.

The oxide layer thickness of NA95 to NA60 decreased from 250 to 60 μm with increasing sialon content. This result also agreed with the oxidation weight gain (Fig. 9). Mullite seems to be a barrier to oxygen diffusion. Fig. 11 shows the bending strengths of the composites at room temperature after oxidation at 1400 °C. The specimens with little oxidation weight gain, NA99–NA80, scarcely exhibited degradation of mechanical strength even after 500 hours of oxidation.

4. Conclusions

Compositions of Al_2O_3, Si_3N_4 and AlN were sintered to produce six different compositions of alumina-sialon composites. The compositions were intended to contain 1.3–79 wt % of sialon, when $z = 2$. All the specimens including pure alumina were sintered under four temperature conditions, reaching the highest density at 1700 °C. The crystalline phases of the sintered compacts consisted of α-alumina and β-sialon, though the z-values and the sialon content shifted to higher values than the nominal ones. The shift was caused by the nitridation of alumina coexisting with Si_3N_4 or sialon. Sialon seems to act as a binder of alumina in the microstructure of composites. It promoted the densification and suppressed the grain

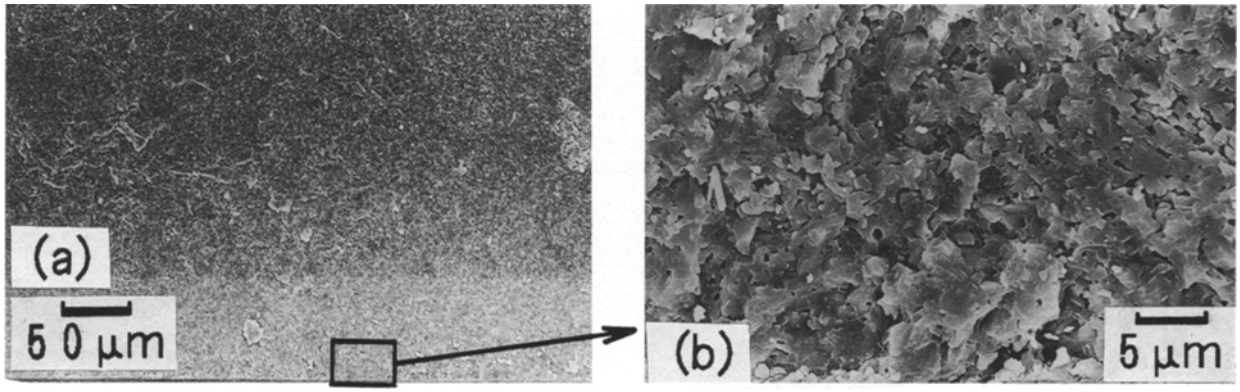

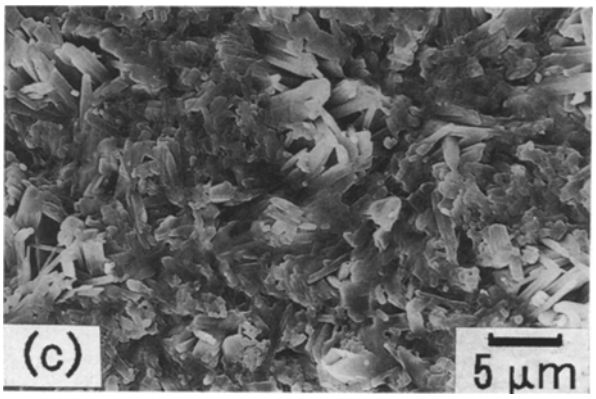

Figure 10 Cross sections of (a) specimen (b) oxidation layer and (c) oxidation surface of NA80 oxidized for 500 hours at 1400 °C.

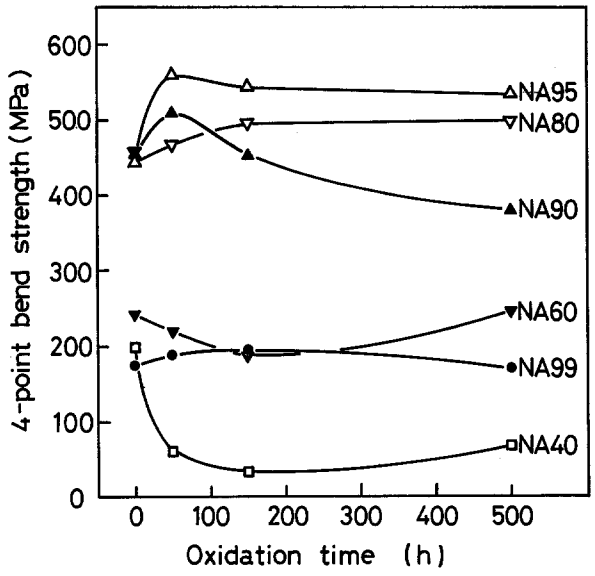

Figure 11 Strength of composites at room temperature after oxidation at 1400 °C.

growth of alumina. The bending strength of the composites was 450 MPa, about twice that of pure alumina produced under the same condition. The strengths at high temperatures also improved with increasing sialon content. The composite with 30 wt % sialon had the maximum K_{IC} of 4.3 MPa·$m^{1/2}$, where a continuous network of intergranular sialon phase was formed. Young's modulus decreased from 400 to 150 GPa with increasing sialon content. This indicates that dense ceramics with a desired Young's modulus can be obtained by appropriate selection of compositions. Oxidation of composites at 1400 °C resulted in small weight gains. A mullite layer was formed on the surface of the composites by the reaction of air, sialon and alumina. The strength of the composites at room temperature after oxidation exhibited little degradation even after 500 hours of oxidation.

Acknowledgement

The author would like to thank Dr O. Kamigaito for his contributions to this work.

References

1. G. DAS, M. G. MENDIRATT and G. R. CORNISH, *J. Mater. Sci.* **17** (1982) 2486.
2. K. TAKATORI and O. KAMIGAITO, *J. Mater. Sci. Lett.* **7** (1988) 1024.
3. K. TAKATORI, H. DOI and O. KAMIGAITO, *J. Mater. Sci.* **3** (1984) 987.
4. Japanese Industrial Standards Committee, Testing Method for Flexural Strength of High Performance Ceramics, *JIS R* 1601.
5. K. NIIHARA, R. MORENA and D. P. H. HASSELMAN, *J. Mater. Sci. Lett.* **1** (1982) 13.

Received 9 July
and accepted 30 October 1990